A New Method of Measuring Velocity Profiles using a Multi-Electrode Electromagnetic Flow Meter

G.P. Lucas[a] and T. Leeungculsatien[a]

[a] School of Computing and Engineering University of Huddersfield, Huddersfield HD1 3DH, UK

E-mail: g.lucas@hud.ac.uk

ABSTRACT

This paper describes a model of a novel design of electromagnetic flow meter for velocity profile measurement in single phase and multiphase flows with non-uniform axial velocity profiles. A simulated Helmholtz coil is used to produce a uniform magnetic field orthogonal to both the flow direction and the plane of an electrode array embedded on the internal surface of a non-conducting pipe wall. Induced voltages acquired from the electrode array are related to the flow velocity distribution via variables known as 'weight values' which are calculated using COMSOL Multiphysics software. Matrix inversion is used to calculate the velocity distribution in the flow cross section from the induced voltages measured at the electrode array. This paper presents simulations including, firstly the effects of the velocity profile on the electrical potential distribution, secondly the induced voltage distribution at the electrode pair locations, and thirdly the reconstructed velocity profile calculated using the weight values and the matrix inversion method mentioned above. The flow pipe cross-section is divided into a number of pixels and the mean flow velocity in each of the pixels is calculated from the measured induced voltages. Reference velocity profiles that have been investigated include a uniform velocity profile and a linear velocity profile. The results show good agreement between the reconstructed and reference velocity profiles. The results presented in this paper are most relevant to flows in which variations in the axial flow velocity occur principally in a single direction.

Helmholtz coil, Induced voltage, Magnetic flux density, Weight value

1 INTRODUCTION

Conventional electromagnetic flow meters (EMFMs) have been used successfully in varieties of industries for measuring volumetric flow rates of conducting fluids in single phase pipe flows. At present, a conventional EMFM can measure the volumetric flow rate of a single phase flow with an error as low as ±0.05% of reading provided that the velocity profile is axisymmetric. However highly non-uniform velocity profiles are often encountered, e.g. just downstream of partially open valves. The axial flow velocity just downstream of a gate valve varies principally in the direction of the valve stem, with the maximum velocities occurring behind the open part of the valve and the minimum velocities behind the closed part of the valve. In such non-uniform velocity profiles the accuracy of the conventional EMFM can be seriously affected (Lim and Chung, 1999) and high accuracy volumetric flow rate measurements can only be achieved by measuring the axial velocity profile and using this to determine the mean flow velocity in the cross section. Large variations in the axial flow velocity can also occur in multiphase flows e.g. horizontal and inclined multiphase flows in which axial velocity variations occur principally in the direction of gravity, with the minimum axial velocity at the lower side of the pipe and the maximum velocity at the upper side of the pipe Lucas, (1995). A specific example of a multiphase which is of great interest to the oil industry is inclined oil-in-water flow. Such flows are 'water continuous' and so the multiphase mixture is electrically conducting allowing the use of electromagnetic flow meters. However the water velocity varies from a minimum at the lower side of the inclined pipe to a maximum at the upper side of the inclined pipe and this causes erroneous readings from a conventional electromagnetic flow meter. In view of the above, the objective of this paper is to describe a new non-intrusive electromagnetic flow metering technique for (i) measuring the axial velocity profile of single phase flows of conducting fluids and (ii) measuring the axial velocity profile of the conducting continuous phase of multiphase mixtures (such as horizontal and inclined oil-in-water flows and solids-in-water flows) in which the conductivity of the dispersed phase is very much lower than the conductivity of the continuous phase. [Note that in a previous paper Wang et al., (2007b) it has been shown that the relatively minor variations of fluid conductivity, which occur in the cross

section of such multiphase flows, have only a minimal effect on the operation of electromagnetic flow meters. This is particularly true if the volume fraction of the non-conducting dispersed phase is less than about 0.4].

An alternative approach to accurate volumetric flow rate measurement in highly non-uniform single phase flows has been proposed by authors such as Horner (1998) who described a six electrode electromagnetic flow meter which is insensitive to the flow velocity profile. However, this type of flow meter does not provide information on the local axial velocity distribution in the flow cross section. This can be a major drawback, particularly in multiphase flows where, for example, the volumetric flow rate of a particular phase can only be found by integrating the product of the local phase velocity and the local phase volume fraction in the flow cross section (the local volume fractions of individual phases can be determined using an auxiliary technique such as Electrical Resistance Tomography). The approach of Horner (1998) would be of no benefit, for example, in determining the water volumetric flow rate in highly inclined solids-in-water flows such as those observed by Lucas et al., (1999).

The essential theory of EMFMs states that charged particles in a conducting material which moves in a magnetic field experience a Lorentz force acting in a direction perpendicular to both the material's motion and the applied magnetic field. Williams (1930) applied a uniform transverse magnetic field perpendicular to the line joining the electrodes and the fluid motion and his experiments revealed that for a uniform velocity profile the flow rate is directly proportional to the voltage measured between the two electrodes. Subsequently Shercliff (1962) showed that the local current density $\mathbf{j}$ in the fluid is governed by Ohm's law in the form of

$$\mathbf{j} = \sigma(\mathbf{E} + \mathbf{v} \times \mathbf{B}) \tag{1}$$

where σ is the local fluid conductivity, $\mathbf{E}$ is the local electric field in the stationary coordinate system, $\mathbf{v}$ is the local fluid velocity, and $\mathbf{B}$ is the local magnetic flux density. The expression $(\mathbf{v} \times \mathbf{B})$ represents the Lorentz force induced by the fluid motion, whereas $\mathbf{E}$ is principally due to charges distributed in and around the fluid. For fluids where the conductivity variations are relatively minor (such as the single phase and multiphase flows under consideration in this paper) Shercliff simplified equation 1 to show that the local potential U in the flow can be obtained by solving

$$\nabla^2 U = \nabla \cdot (\mathbf{v} \times \mathbf{B}) \tag{2}$$

For a pipe flow in which the flow cross section is divided into N pixels and where N potential difference measurements are made between electrodes placed around the internal circumference of the pipe a solution to equation 2 is of the form

$$U_j = \frac{2\overline{B}}{\pi a} \sum_{i=1}^{N} v_i w_{ij} A_i \tag{3}$$

where A_i represents the cross sectional area of the ith of N pixels into which the flow cross section is divided, v_i is the mean axial flow velocity in the ith pixel and U_j is the jth of N potential difference measurements made at the boundary of the flow. The term w_{ij} is a so called weight value (after Shercliff (1962)) which relates the flow velocity in the ith pixel to the jth potential difference measurement, a is the internal pipe radius and $\overline{B}$ is the mean magnetic flux density in the flow cross section. It will be shown later in this paper that equation 3 can be manipulated to enable the local axial flow velocity in each of the N pixels to be determined from N potential difference measurements U_j made on the boundary of the flow.

In section 2 of this paper it is shown how the weight values w_{ij} can be calculated, for a particular magnetic flow meter geometry, using an 'electromagnetics' software package such as COMSOL. In

section 3 values of U_j are calculated for a number of different simulated velocity profiles in the EMFM. In section 4 of the paper, a reconstruction technique is outlined which enables the pixel velocities v_i to be determined from the weight values w_{ij} and the boundary voltage measurements U_j.

2 NUMERICAL MODELLING OF ELECTROMAGNETIC FLOWMETER

2.1   Electromagnetic Flow Meter Geometry

An electromagnetic flow meter was modelled using COMSOL Multiphysics software. The specification of the EMFM was that it consisted of a PTFE (polytetrafluoroethylene) flow pipe mounted within Helmholtz coils. The EMFM contained 16 equispaced electrodes located at the plane $z = 0$. The inner diameter of the flow pipe was 0.08m, the outer diameter was 0.09m and its axial length was 0.3m. The inner and outer diameters of the two coils were 0.2048m and 0.2550m respectively (refer to Figure 1(a)). A cylindrical domain with a diameter of 0.32m and a length of 0.32m represents the boundary of the computing domain (refer to Figure 1).
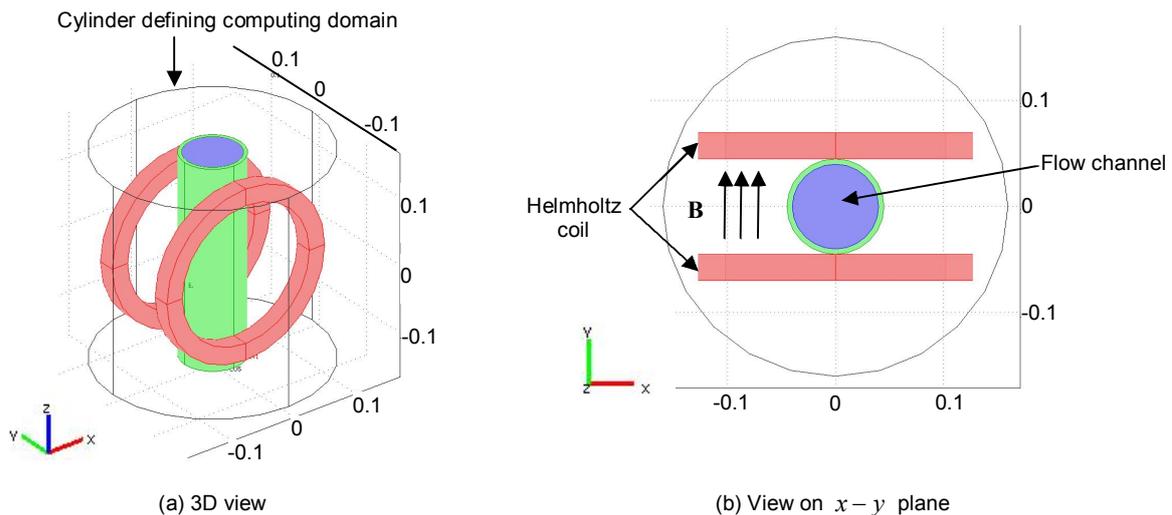

(a) 3D view   (b) View on $x - y$ plane

Figure 1: Schematic diagram of the electromagnetic flow meter used in the simulation

In order to calculate the relevant weight values (see section 1) potential difference measurements must be acquired from electrode pairs at the internal boundary of the flow pipe (at the plane $z = 0$), these electrodes being in contact with the flowing medium. Sixteen electrodes were placed at angular intervals of 22.5 degrees on the flow pipe boundary (refer to Figure 2) the electrodes being denoted e1, e2 etc, with electrode e5 at the top of the flow cross section and electrode e13 at the bottom of the flow cross section (Figure 2). For the simple flow meter geometry described in this paper the flow cross section was divided into seven pixels. The geometry of these seven pixels was chosen such that the chords joining seven pairs of electrodes were located at the geometric centres (in the y direction) of the pixels (refer to Figure 2). The fluid pixels are categorized as pixel 1 at the top of the flow cross section to pixel 7 at the bottom of the flow cross section. This pixel arrangement was chosen because, as described in section 1, variations in the axial velocity in many flows of interest tend to occur in a single direction. Thus, for measuring the velocity profile behind a partially open gate valve, the flow meter would be orientated such that the line joining e13 to e5 would be parallel to the valve stem (i.e. the direction of the magnetic field would be parallel to the valve stem). For making measurements in horizontal or inclined oil-in-water flows the line joining e13 to e5 would be parallel to the direction of gravity (i.e. the direction of the magnetic field would be parallel to the direction of gravity). The pixel areas A_i are shown in Table 1. In the simulations described in this paper, for each simulated flow condition investigated, seven potential difference measurements were made between the seven electrode pairs shown in table 1 (the jth potential difference measurement U_j was made between the

j^{th} electrode pair shown in table 1). The local magnetic flux density $\mathbf{B}$ was perpendicular to both the fluid direction and to the chords joining the electrode pairs (Figure 2).

Note that the fluid conductivity used in the simulations was $1.5 \times 10^{-2}\,\mathrm{Sm}^{-1}$, this conductivity value is typical of the mains water in northern England. In addition the flow pipe was assumed to be made of PTFE with conductivity of $1 \times 10^{-15}\,\mathrm{Sm}^{-1}$, and the Helmholtz coil material was assumed to be copper with a conductivity of $5.96 \times 10^{7}\,\mathrm{Sm}^{-1}$. The imposed current in the Helmholtz coil generated a magnetic field of mean strength $\overline{B}$ equal to $7.996 \times 10^{-4}\,\mathrm{T}$ (7.996 gauss) as described in section 2.2 below.

It should also be noted that for a sixteen electrode system, such as that shown in figure 2, up to fifteen independent potential difference measurements can be made. With reference to the techniques described in sections 1 and 4 of this paper, this would allow the flow velocity to be determined in up to 15 pixels into which the flow cross section is divided. The sizes and shapes of these 15 pixels could be selected as required (provided that the relevant weight functions relating the pixel velocities to the boundary potential difference measurements are calculated). If the variation of the axial velocity was unlikely to be in a single direction then instead of using the pixel arrangement shown in figure 2, the use of pixels of approximately square shape would be more appropriate. Note also that although in the study described in this paper electrodes e13 and e5 are not used, they would be required if additional pixels were used as described above.
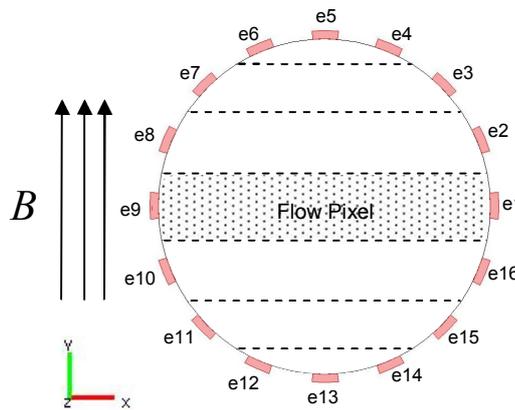

Figure 2: Schematic diagram of the flow pixels

Table 1: Electromagnetic flow meter geometries

Area A_i (m^2)		Electrode pair U_j	
Pixel1 (i=1)	1.738e^{-4}	Pair 1 (j=1)	e4 – e6
Pixel2 (i=2)	6.267e^{-4}	Pair 2 (j=2)	e3 – e7
Pixel3 (i=3)	1.077e^{-3}	Pair 3 (j=3)	e2 – e8
Pixel4 (i=4)	1.264e^{-3}	Pair 4 (j=4)	e1 – e9
Pixel5 (i=5)	1.077e^{-3}	Pair 5 (j=5)	e16 – e10
Pixel6 (i=6)	6.267e^{-4}	Pair 6 (j=6)	e15 – e11
Pixel7 (i=7)	1.738e^{-4}	Pair 7 (j=7)	e14 – e12
(a) Pixel areas		(b) Electrode pair	

2.2   Simulated Magnetic Flux Density Distribution

In the current investigation the Helmholtz coil which was used to produce a nearly uniform local magnetic flux density distribution is described in greater detail in a previous paper Leeungculsatien et al., (2009). A brief overview of the numerical modelling setup for the EMFM follows below. All the numerical simulations were carried out using the commercial finite element analysis software package known as COMSOL Multiphysics (COMSOL, (2005)). The EMFM was investigated using the COMSOL 'Electric and Induction Currents' application mode with the 'time-harmonic stationary linear solver' contained in the COMSOL 'AC/DC' module. This solver calculates the distributions of the local magnetic flux density $\mathbf{B}$ and the local electrical potential V in the computing domain.

A Helmholtz coil consists of two identical circular coils. In the EMFM design these coils were placed symmetrically on each side of the PTFE flow pipe as shown in figure 1. The coils were simulated such that the current flows through both coils in the same direction and each coil carries an equal amount of electric current giving rise to a relatively uniform magnetic flux density distribution in the flow cross section. The simulated magnitude of the magnetic flux density in the y direction is relatively constant and has a maximum value of 7.757×10^{-4} T and minimum value of 8.044×10^{-4} T in the flow cross section. The mean value $\overline{B}$ of the magnitude of the y component of the magnetic flux density in the flow cross section was 7.996×10^{-4} T (7.996 gauss).

2.3 Calculation of the Weight Values

To numerically simulate the weight value w_{ij}, which relates the mean flow velocity v_i in the ith pixel to the jth potential difference measurement U_j, the flow channel is divided into seven pixels as described above (refer to figure 2). The condition of the simulation is that the fluid in the pixel for which weight values are to be calculated is given a flow velocity of greater than zero in the z direction whilst the remaining pixels all have zero fluid velocity. Figure 3 shows the distribution of the Lorentz forces and the induced electrical potentials when the fluid in pixel 4 has an imposed velocity in the z direction while the fluid in the remaining fluid pixels is at rest. Figure 3(a) illustrates the Lorentz force distribution arising from the imposed velocity in pixel 4. The magnetic field interacts with the charges carried in the water via these Lorentz forces causing the separation of charged ions (positive and negative) and giving rise to the electrical potential distribution shown in figure 3(b). The arrows shown in figure 3(a) also represent the direction of the local induced current density and it can be seen that for the (highly contrived) case in which flow occurs in pixel 4 only there is circulation of the electric current.
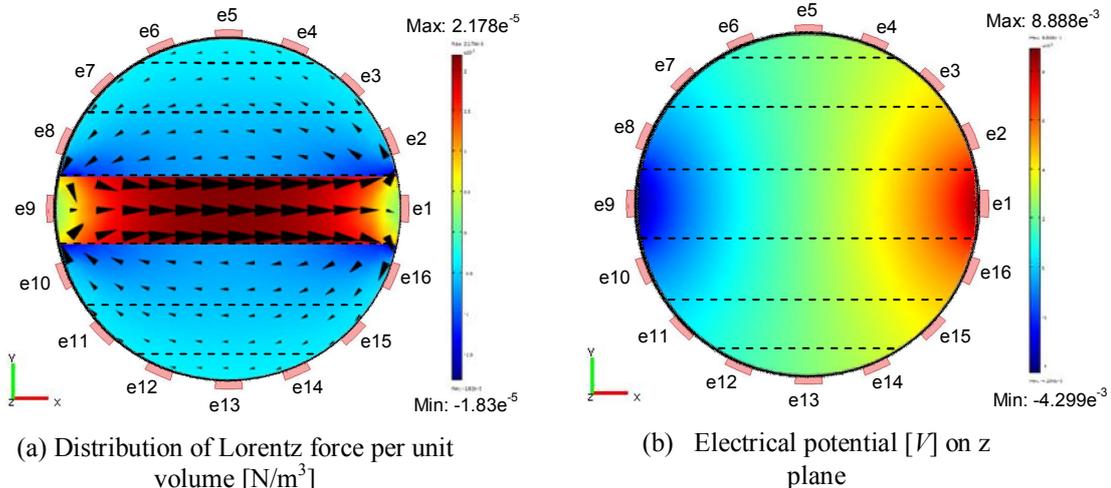

(a) Distribution of Lorentz force per unit volume [N/m^3]

(b) Electrical potential [V] on z plane

Figure 3: Fluid pixel 4 simulation

From the potential distribution given in Figure 3(b) the seven potential differences U_j between the 7 electrode pairs given in Table 1 can be calculated allowing all of the weight values w_{4j} associated with pixel 4 to be calculated according to equation 4 (with $i = 4$ and $j = 1$ to 7). The process is then repeated for each of the other six pixels in succession until all relevant 49 weight values have been calculated. Figure 4(a) shows the induced voltages plotted against electrode pairs for all of the seven simulations. [Note that the very large simulated pixel velocity of $500\,\text{ms}^{-1}$ was used to obtain the

results shown in Figures 3 and 4 to improve the accuracy of the weight values calculated using COMSOL]. Figure 4(b) shows the 49 weight values calculated from the induced voltages given in Figure 4(a) by using equation 4.

$$w_{ij} = U_j \frac{\pi a}{2\bar{\bar{B}}} \frac{1}{v_i A_i} \tag{4}$$
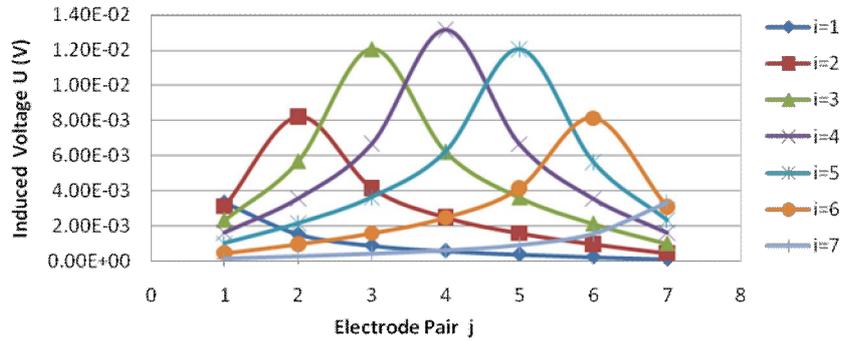
(a) Induced voltage distribution
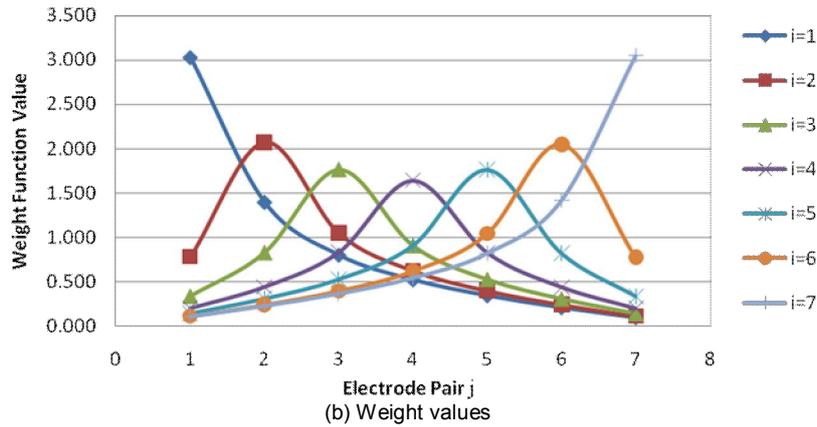
(b) Weight values

Figure 4: Weight values calculation

3 EFFECT OF VELOCITY PROFILE ON ELECTRICAL POTENTIAL DISTRIBUTION

The next stages of the investigation were; (i) to apply different simulated velocity profiles to the flowing fluid; (ii) to find the resultant induced potential differences U_j using COMSOL; (iii) to reconstruct the velocity profiles using equation 6; and (iv) to compare the reconstructed velocity profiles with the applied simulated velocity profiles. Two different simulated velocity profiles were investigated, a uniform velocity distribution and a linear velocity distribution as described below.
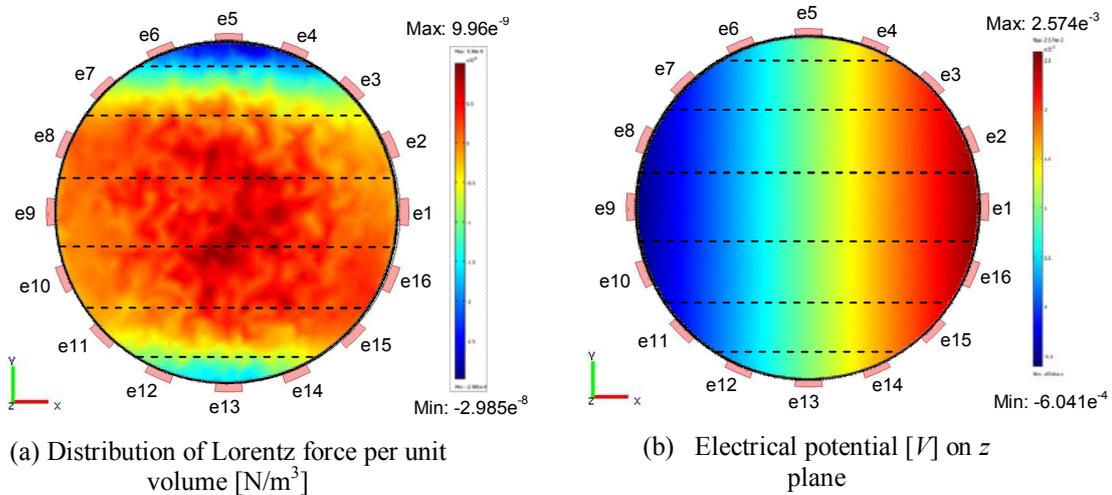
3.1 Uniform Velocity Profile

(a) Distribution of Lorentz force per unit volume [N/m^3]

(b) Electrical potential [V] on z plane

Figure 5: Uniform velocity profile

Figure 5 shows the effect of an imposed uniform velocity distribution of $50\mathrm{ms}^{-1}$ in the flow cross section on the Lorentz force distribution and the electrical potential distribution. The authors acknowledge that this velocity profile is unrealistic because (i) fully developed turbulent flows in circular pipes are generally axisymmetric with '1/7th power law' velocity profiles and (ii) the magnitude of the velocity is unrealistic. Nevertheless, as a means of investigating flow velocity image reconstruction techniques this uniform velocity profile is very useful in its simplicity.

3.2 Linear Velocity Profile

(a) Distribution of Lorentz force per unit volume [N/m^3]
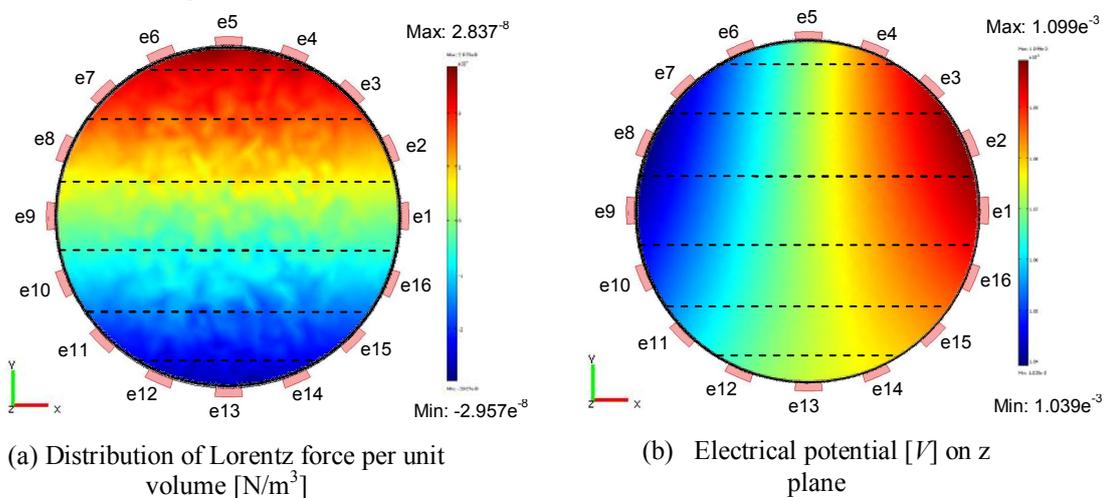
(b) Electrical potential [V] on z plane

Figure 6: Linear velocity profile

Figure 6 shows the effect of an imposed linear velocity distribution in the flow cross section on the Lorentz force distribution and the electrical potential distribution. The flow velocity v_z in the z direction is given by the expression

$$v_z = 1 + \left(\frac{y}{a}\right) \qquad (5)$$

where y is the coordinate in the simulation and a is the internal pipe radius. This results in v_z varying linearly from zero at $y = -0.04\,\text{m}$ to $2\,\text{ms}^{-1}$ at $y = 0.04\,\text{m}$. This type of linear velocity profile can occur in inclined multiphase flows as observed by Lucas et al (1999) (see above).

The relevant induced voltages U_j for the uniform velocity profile and linear velocity profile were calculated for the electrode pairs shown in Table 1. It should be noted that the electrical potential distribution for the uniform velocity profile and linear velocity profile are entirely different from each other. For the uniform velocity distribution the induced voltages between pairs 1, 2 and 3 are the same as for pairs 7, 6, and 5 are respectively. For the linear velocity profile the induced voltage between pair 1 is higher than that for pair 7. Similarly the induced voltages between pairs 2 and 3 are respectively higher than for pairs 6 and 5. Moreover for the linear velocity profile the highest induced potential is between electrode pair 3 while the maximum induced voltage for the uniform velocity profile is between electrode pair 4. Similar relationships between the velocity profile and the induced voltage distribution have also been previously observed Wang et al., (2007b).

4 RECONSTRUCTION METHOD

As mentioned earlier the weight values w_{ij} are used to reconstruct the mean velocity v_i in each pixel using the calculated induced voltages U_j. The reconstruction method can be expressed simply by the following matrix equation

$$\mathbf{V} = \frac{\pi a}{2\overline{B}}[\mathbf{WA}]^{-1}\mathbf{U} \qquad (6)$$

In which $\mathbf{V}$ is a single column matrix containing the pixel velocities v_i, $\mathbf{W}$ is a square matrix containing the relevant weight values w_{ij}, $\mathbf{A}$ is a single matrix containing information on the pixel areas A_i and $\mathbf{U}$ is a single column matrix containing the calculated potential differences U_j for a given imposed velocity profile.

(a) Reconstructed uniform velocity profile   (b) Reconstructed linear velocity profile
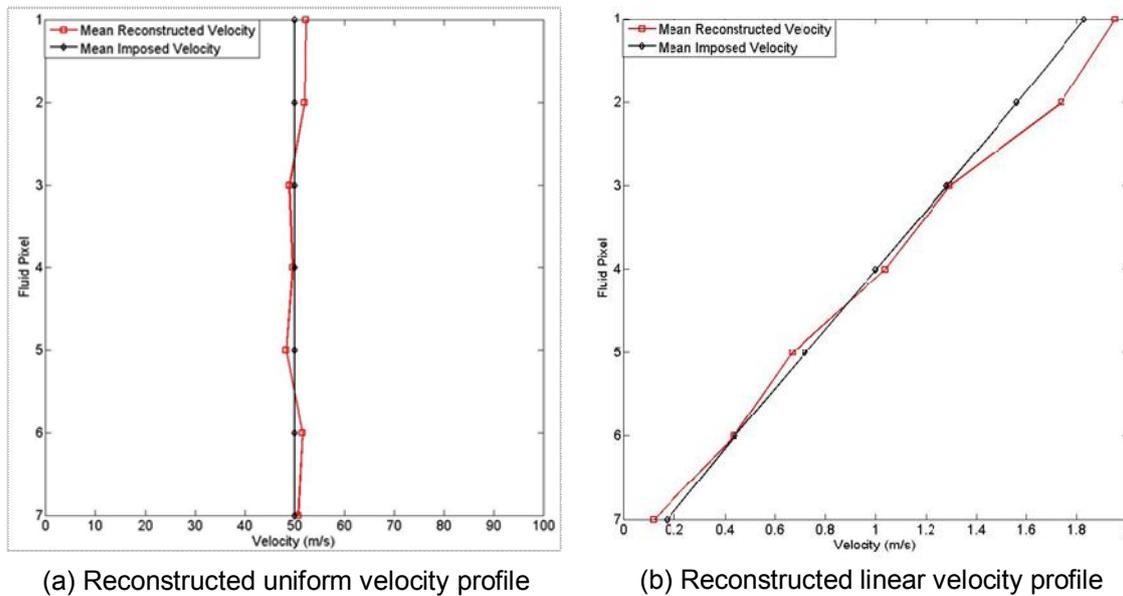
Figure 7: Reconstructed velocity

For the two velocity profile simulations that were undertaken the reconstructed velocity profiles are shown in Figures 7(a) and 7(b). Also shown in Figures 7(a) and 7(b) are the original imposed velocity

profiles from which the potential difference measurements U_j were obtained. With close inspection of Figure 7 it can be seen that the reconstructed velocity profiles have excellent agreement with the original imposed velocity profiles for both the uniform and linear velocity profiles. Figure 7(a) shows that for the imposed uniform velocity profile the maximum (most overestimated) and minimum (most under estimated) reconstruction errors occur in pixel 1 ($+4.565\%$) and pixel 5 (-3.33%) respectively. The most accurate reconstructed velocity is in pixel 4 with an error of only 0.722%. The linear velocity profile has maximum and minimum reconstruction errors in pixels 2 and 7 respectively. The most accurate reconstructed velocities for the linear velocity profile are in pixels 3 and 6 with errors of $+0.912\%$ and -0.797% respectively.

The total volumetric flow rate Q_w of the liquid can be calculated from the reconstructed velocity profile as follows;

$$Q_w = \sum_{i=1}^{7} A_i v_i \tag{7}$$

in which Q_w is the water volumetric flow rate, A_i is the area of the ith pixel, and v_i is the reconstructed velocity in the ith pixel. Let the true volumetric flow rate associated with the imposed uniform velocity profile be Q_{wiu} and the volumetric flow rate associated with the reconstructed uniform velocity profile be Q_{wru}. Also let the true volumetric flow rate associated with the imposed linear velocity profile be Q_{wil} and the volumetric flow rate associated with the reconstructed linear velocity profile be Q_{wrl}.

For the uniform velocity profile Q_{wiu} is calculated to be $2.509 \times 10^{-1} \text{m}^3 \text{s}^{-1}$ and Q_{wru} is found to be $2.503 \times 10^{-1} \text{m}^3 \text{s}^{-1}$. There is thus an error of only -0.238% in the total volumetric flow rate obtained from the reconstructed uniform velocity profile.

For the linear velocity profile Q_{wil} is calculated to be $5.026 \times 10^{-3} \text{m}^3 \text{s}^{-1}$, and Q_{wrl} is calculated to be $5.147 \times 10^{-3} \text{m}^3 \text{s}^{-1}$. There is thus an error of only $+2.413\%$ in the total volumetric flow rate obtained from the linear velocity profile. It is believed that this error could be reduced by using a greater number of pixels.

5 CONCLUSIONS

This paper describes a new measuring technique for mapping velocity profiles in single phase and multiphase flows. The results described in this paper are mainly relevant to flows in which the axial flow velocity varies *principally* in a single direction such as (i) flows behind partially open valves or (ii) horizontal and inclined multiphase flows in which the continuous phase is electrically conducting. However by using alternative pixel arrangements the technique can be readily adapted to flows in which the axial velocity profile variation is not principally in a single direction. The paper has demonstrated the Lorentz force distributions and induced electrical potential distributions associated with uniform and linear imposed velocity profiles. A weight value theory for an electromagnetic flow meter with multiple electrodes has been implemented and proved to be a valid method for relating the mean flow velocity in a pixel to the potential differences measured between various pairs of electrodes. Moreover, this paper has used a matrix inversion method that can be combined with the weight values to reconstruct the mean velocity in each of a number of pixels from a given set of boundary potential difference measurements. These reconstructed velocities give good agreement with the reference pixel velocities. The reconstructed velocity profiles enable reasonably accurate volumetric flow estimates to be made, provided that the variations in the axial velocity occur principally in the direction of the magnetic field.

6 REFERENCES

COMSOL, C. (2005) *COMSOL Corporation Femlab 3.3 user's guide*.

HONER, B. (1998) A novel profile-insensitive multi-electrode induction flowmeter suitable for industrial use. *Meas. Sic. Technol.,* 24**,** 131-137.

LEEUNGCULSATIEN, T., LUCAS, G. P. & ZHAO, X. (2009) A numerical approach to determine the magnetic field distribution of an electromagnetic flow meter. *School of Computing and Engineering Researchers' Conference, University of Huddersfield***,** 147-152.

LIM, K. W. & CHUNG, M. K. (1999) Numerical investigation on the installation effects of electromagnetic flowmeternext term downstream of a 90° elbow–laminar flow case. *Flow. Meas. Instrum.,* 10**,** 167-174.

LUCAS, G. P., CORY, J., WATERFALL, R. C., LOH, W. W. & DICKIN, F. J. (1999) Measurement of the solids volume fraction and velocity distribution in solids-liquid flows using dual-plane ERT Flow. *Meas. Instrum.,* 10**,** 249-258.

LUCAS, G. P., WANG, M., MISHRA, R., DAI, Y. & PANAYOTOPOULOS, N. (2004) Quantitative comparison of gas velocity and volume fraction profiles obtained from a dual-plane ERT system with profiles obtained from a local dual-sensor conductance probe, in a bubbly gas–liquid flow. *3rd international symposium on process tomography in Poland.*

LUCAS, G. P. (1995) Modelling velocity profiles in inclined multiphase flow to provide a priori information for flow imaging. *Chemical Engineering Journal,* 56**,** 167–173.

SHERCLIFF, J. A. (1962) the Theory of Electromagnetic Flow-Measurement. UK.

WANG, J. Z., LUCAS, G. P. & TIAN, G. Y. (2007a) A numerical approach to the determination of electromagnetic flow meter weight function. *Meas. Sic. Technol.,* 18**,** 548-554.

WANG, J. Z., TAIN, G. Y. & LUCAS, G. P. (2007b) Relationship between velocity profile and distribution of induced potential for an electromagnetic flow meter *Flow. Meas. Instrum. ,* 18**,** 99-105.

WILLIAMS, E. J. (1930) The introduction of electromotive forces in a moving liquid by a magnetic field, and its application to an investigation of the flow of liquids. *Proc Phys Soc* A42**,** 466-487.